Journal of Materials Chemistry A

Accepted Manuscript

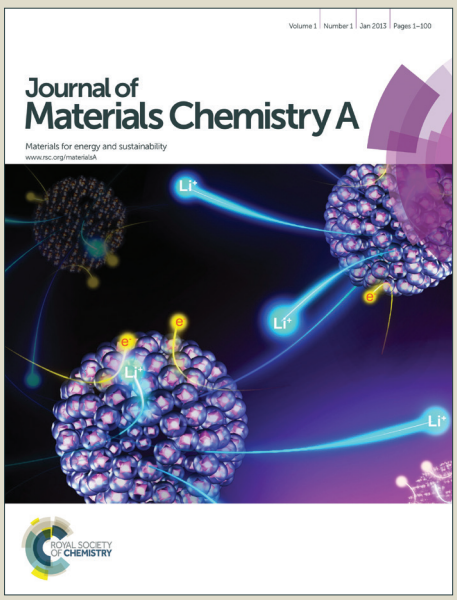

ROYAL SOCIETY OF CHEMISTRY

www.rsc.org/materialsA

Journal of Materials Chemistry A RSCPublishing

PAPER

Effective Strategies for Improving Electrochemical Properties of Highly Porous Si Foam Anodes in Lithium-Ion Batteries

Cite this: DOI: 10.1039/x0xx00000x

Received 00th January 2012,
Accepted 00th January 2012

DOI: 10.1039/x0xx00000x

www.rsc.org/

Taesoo Bok,[a] Sinho Choi,[a] Jeongchan Lee,[b] and Soojin Park*[a]

We describe effective strategies to enhance the electrochemical performance of highly porous silicon anode using well-known magnesiothermic reduction. Highly porous silica is synthesized by combining a triblock copolymer template and silicon precursor. Subsequent magnesiothermic reduction of the porous silica leads to a conversion of silica to silicon particles without a significant change of original silica structure. In addition, we employ sodium chloride as a heat scavenger to reduce an exothermic reaction that occurs during the magnesiothermic reaction of silica. Since the fusion of sodium chloride absorbs the exothermal heat, as-synthesized porous silicon can remain the original silica structure without aggregation. The final strategy is to improve the electrical conductivity of Si particles by introducing metal particles during the magnesiothermic reaction, resulting in a significant improvement of electrochemical performance including a cycling retention and initial coulombic efficiency. These approaches may be extended to ameliorate other anode materials for practical lithium-ion battery applications.

1. Introduction

Currently, rechargeable lithium-ion batteries (LIBs) are the dominant power sources for medical and portable electronic devices, such as laptop computers, mobile phones, camcorders, and radio frequency identification.[1-3] Furthermore, the development of next-generation LIBs with high energy density and long cycle life is of great technological importance to be used in hybrid vehicles, plug-in hybrid vehicles, electric vehicles, and renewable energy storage system[4-6]. To meet the requirements of next-generation LIBs, the electrode materials must have high specific gravimetric/volumetric capacities, a high power density, and a long cycling life.[4-6]

The increasing demand for high-performance LIBs has driven intense interest in developing significantly improved electrode materials. At present, various carbonaceous anode materials have been used in commercial LIBs, however, the low theoretical capacity (372 mAh g^{-1}) cannot satisfy the demand of next-generation LIBs.[7, 8] Among the available candidate materials exhibiting a high storage capacity, silicon (Si) is the most promising anode material owing to its high theoretical capacity (4200 mAh g^{-1}, an order magnitude higher than that of graphite), relatively low working potential (<0.5 V vs. Li/Li^+), natural abundance, and environmentally friendliness.[9] Even though Si anode materials have many advantages mentioned above, it has a fatal weakness for the practical application in LIBs. The major drawback of Si anode is a large volume change (>300%) that occurs during lithiation and delithiation process. The repeated cycling can generate an enormous mechanical stress within the Si material, leading to severe cracking and pulverization of the electrode. Consequently, the Si electrode results in a significant capacity fading due to the electrical disconnection of the electrode from the current collector.[10] Other disadvantages of the Si anode are low intrinsic electrical conductivity and low lithium diffusion rate.[11, 12]

In order to solve the problems related to Si anodes, great efforts have been devoted to mitigating the pulverization of Si and enhancing electrical conductivity of Si by developing several strategies, including nanostructuring (e.g., nanoparticles, nanowires, nanotubes, hollow spheres), porous structures, nanocomposites, coating of Si active materials with conductive materials (e.g., carbon, graphene, carbon nanotubes, metals, conducting polymers), application of electrolyte additive, and synthesis of new binders.[13-20] Nanostructured Si have been used to reduce mechanical stress that occurs during cycling, resulting in accommodation of a large volume change of Si, which in turn significantly improved a long-term cyclability. It also provides other benefits, including short Li-ion diffusion length within the electrode and improved rate capability due to the large surface area, compared to micron-sized Si.[21,22] However, nanostructured Si faces some challenges to be solved. Nano-sized Si with high surface area shows undesired side-reaction on the Si surface, thermal runaway, and low volumetric energy density, which are obstacles for practical LIB applications.[21, 22]

To solve these critical issues, one of the best solutions is to combine micro- and nano-scale materials to capitalize on advantages and restrain drawbacks of the two components. Several examples have been reported including nanostructuring of micrometer-sized Si particles, dispersion of nano-sized Si in carbon matrix, self-assembly of nanoscale Si and carbon, template-based chemical synthesis of porous Si, three-dimensionally (3D) interconnection of one-dimensional Si structures.[23-27] Among these approaches, porous Si structure has been proven to be highly efficient as follows: (i) void space of the pores accommodates a volume expansion to reduce the mechanical stress during cycling, resulting in attainment of a stable cycling and (ii) porous regions increase the accessibility of electrolyte and lithium ions to shorten lithium ion diffusion distance within the electrodes, leading to a high rate capability.[28-31]

For example, Kim et al. synthesized a 3D macroporous Si using silica (SiO_2) particle template which exhibited a reversible specific

capacity of 2800 mAh g^{-1} at 1 C rate with excellent cycling performance (capacity retention of 90% at 1 C rate after 100 cycles). However, the high-cost and low yield (~5%) synthetic process may hinder its large scale production.[26] Recently, Jia et al. prepared a 3D mesoporous Si material with a lotus-like morphology using a magnesiothermic reduction method. Subsequent carbon-coated mesoporous Si composite showed a stable capacity of ~1500 mAh g^{-1} for 100 cycles at 1 C rate and a high rate capability up to 15 C rate. However, the existence of numerous mesopores may induce a serious side-reaction and may not effectively accommodate a large volume expansion during cycling.[31]

Herein, we demonstrate facile, inexpensive, and effective strategies to enhance the electrochemical performances of highly porous Si foam anode in lithium-ion batteries. Firstly, we synthesize a hierarchical Si foam structure via a magnesiothermic reduction of micrometer-sized SiO_2 foam particles obtained by controlling calcination process. Secondly, we introduce a heat scavenging molten salt during the chemical reduction reaction to minimize exothermic heat, leading to a successful synthesis of shape-preserving Si foam particles. Thirdly, electrically conductive metal nanoparticles are introduced within Si foam particles, and subsequent chemical reduction process leads to a formation of metal-doped Si foam particles. The Si foam anodes obtained by these strategies exhibit a high reversible capacity (>1500 mAh g^{-1}) and a highly stable cycling retention (> 90% after 100 cycles at 0.2 C rate).

2. Experimental

2.1. Preparation of highly porous Silica foam

Silica foam was prepared according to the previously reported method.[32] Typically, 4 g of poly(ethylene oxide)-b-poly(propylene oxide)-b-poly(ethylene oxide) (PEO-b-PPO-b-PEO) triblock copolymer (Pluronic P123, Sigma-Aldrich), a polymer template, was dissolved in 150 ml of 1.6 M HCl solution at 35 ^oC. 4 g of 1,3,5-trimethylbenzene (Mesitylene, Sigma-Aldrich), a swelling agent, was added into the solution containing the copolymer template. The mixed solution was then slowly added into 8.5 g of tetraethylorthosilicate (TEOS, Sigma-Aldrich), a silica precursor. The resulting solution was vigorously stirred for 24 h, and then it was maintained at 80 ^oC for 24 h. Finally, the solid product was filtered and dried at room temperature. As-prepared silica/polymer product was divided into three alumina boat to be calcined to make hierarchical silica particles. To control the amount of residual carbon after calcination, we used three different calcination processes (first portion: no calcination, second portion: 600 ^oC for 2 h in ambient, and third portion: 600 ^oC for 5 h in oxygen environment). Subsequently, three different silica samples were reacted with Mg vapor via magnesiothermic reduction at 700 ^oC for 3 h in an argon-filled alumina vessel to make porous Si particles.

2.2. Characterization of silica and Si foam particles

Microstructure of as-synthesized silica foam and converted Si foam particles were investigated by a normal X-ray diffractometer (Bruker D8 Advance). The internal morphologies of the silica and the Si foam were analyzed by transmission electron microscopy (TEM, JEM-1400) at an acceleration voltage of 120 kV. For the TEM measurement, the silica and Si particles were dispersed in ethanol, then transferred on to a Formvar-coated copper grid. The surface morphologies of the silica and Si foam were characterized by a scanning electron microscopy (Cold FE-SEM S-4800, Hitachi) operating at 10 kV without any metal coating process. The nitrogen adsorption and desorption isotherms were measured with a VELSORP-mini II (BEL Japan, Inc.) at 77 K in the relative pressure range of P/P0 from 0.05 to 0.3. It was fitted to the Brunauer-Emmett-Teller (BET) equation to determine the BET surface areas.

2.3. Electrochemical properties of Si foam anodes

The electrochemical properties of Si foam anode were tested by galvanostatic discharging (lithiation) and charging (delithiation) in coin-type half cells (2016 R-type). The cells that are made up of Si foam/poly(acrylic acid) (PAA, Aldrich) and sodium carboxymethyl cellulose (CMC, Aldrich)/acetylene black composites as working electrode, and lithium metal as the counter electrode, were prepared in a glove box filed argon gas. The electrodes were composed of Si active material (70 wt%), Super-P (10 wt%), and a PAA/CMC (50/50, wt/wt) binder (20 wt%). The resulting slurry was spread on a copper current collector and dried in a vacuum oven at 150 ^oC for 2 h. The electrolyte was composed of 1.3 M $LiPF_6$ in a mixture of ethylene carbonate/diethylcarbonate (Panaxetec, EC/DEC, 30/70 vol%) with an additive of 10 wt% fluoroethylene carbonate (FEC). The loading mass of active materials is in the range of 1.2-1.5 mg cm^{-2}. All cells were cycled at a rate of 0.05-0.5 C in the range of 0.005-1.2 V. All the electrochemical measurements were carried out with a WBCS-3000 battery cycler (Wonatech Co.) at room temperature.

3. Results and discussion

3.1. Conversion of hierarchical SiO_2 foam to Si foam

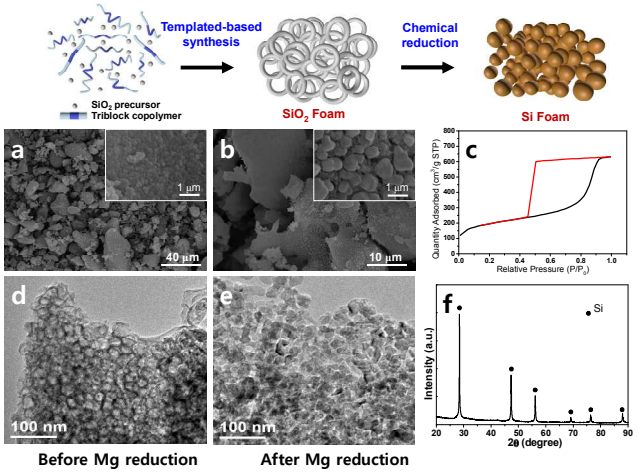

Fig. 1 Top: schematic illustration showing synthetic process of SiO_2 foam and shape-preserving Si. Bottom: (a) low-magnified SEM image (inset: high-magnified SEM) and (d) TEM image of SiO_2 foam prepared by block copolymer template. (b) low-magnified SEM image (inset: high-magnified SEM) and (e) TEM image of Si foam prepared by magnesiothermic reaction of SiO_2. (c) BET plot of the SiO_2 foam shows typical mesoporous structure. (f) XRD pattern of as-synthesized Si foam clearly shows crystalline structure.

Porous SiO_2 particles have been synthesized from self-assembled block copolymer template and silica precursors.[33-35] They have attracted much attention in numerous applications, like adsorption, separation, bio-sensing, catalysis, and Si source materials, owing to their unique porous structures.[36-39] In particular, the porous structures with a high surface area make them well suitable for making porous Si particles via a metallothermic reduction process.

In this study, we prepared sponge-like SiO_2 particles with tens-of-nanometer pores and tens-of-micrometer size using triblock

copolymer as a structure-directing agent and trimethylbenzene as pore expander. When as-prepared SiO_2 particles were reacted with Mg vapor at 700 ^oC (well above the melting temperature of Mg) for 3h, shape-preserving Si particles were obtained.

Figure 1a shows scanning electron microscopy (SEM) image of as-prepared SiO_2 particles. Hundreds-of-nanometer-sized primary SiO_2 particles were aggregated to make micrometer-sized secondary SiO_2 particles (the inset of Figure 1a). Internal morphology of primary SiO_2 particles was characterized by transmission electron microscopy (TEM). The primary SiO_2 particles showed sponge-like structures consisting of a very thin SiO_2 frame and macro-pores (Figure 1d). The nitrogen adsorption isotherm of sponge-like SiO_2 powder is shown in Figure 1c. Brunauer-Emmett-Teller (BET) surface area of the SiO_2 particles was 686.17 m^2 g^{-1}, indicating a high specific surface area.

During the magnesiothermic reduction reaction, porous Si is formed via the solid-state redox reaction between SiO_2 and Mg, $SiO_2(s) + 2Mg(g) \rightarrow Si(s) + 2MgO(s)$.[39] It is well-known that MgO by-products can be removed easily with a concentrated HCl solution. After the chemical reduction of the SiO_2 particles, SEM image of as-synthesized Si particles shows that primary Si particles are aggregated to make tens-of-micrometer-sized secondary particles (Figure 1b). The primary Si particles become bigger compared to original primary SiO_2 particles (Inset of Figure 1b). It may be attributed to the aggregation of Si by an exothermic heat that occurs during the magnesiothermic reaction. However, the dimension of secondary Si particles is similar with that of the original SiO_2 particles. TEM image of primary Si particles shows that crystalline Si particles with 10-20 nm feature size are connected each other with a void space and look like Si foam structures (Figure 1e). After the magnesiothermic reaction, a void space was significantly decreased. However, void regions uniformly distributed within the primary Si particles would be helpful to accommodate a large volume change of Si anode during lithiation and delithiation process. X-ray diffraction (XRD) patterns of as-synthesized Si particles indicate that a highly crystalline Si was successfully obtained from chemical reduction of SiO_2 particle (Figure 1f).

Prior to electrochemical tests of Si foam particles, we synthesized three different Si particles by changing calcination process of copolymer-containing porous SiO_2 particles. Three samples are no calcination, calcination in ambient air, and calcination in oxygen, respectively. All three samples are sponge-like structures regardless of calcination condition, as shown in TEM images (ESI, Figure S1a-S1c). However, BET surface areas of three SiO_2 particles are totally different due to the residual polymer after calcination (ESI, Figure S1d-S1e). These three SiO_2 particles were converted to Si particles via a magnesiothermic reaction at the same condition. Subsequently, as-synthesized Si particles were carbon-coated with carbon contents of 8 wt% using thermal decomposition of acetylene gas at 900 ^oC for 10 min, since pristine Si particles exhibit intrinsically low electrical conductivity. Raman spectrum of the carbon-coated Si particles shows two peaks at ~1360 and ~1580 cm^{-1} corresponding to the disordered band (D band) and the graphene band (G band), respectively. The ratio of the D band to the G band was estimated to be 2.21, indicating an amorphous carbon structure.[23] Intense Raman scattering peaks of pristine Si without carbon layers appear at ~520 cm^{-1} indicating crystalline Si structure, as manifested by above XRD patterns (ESI, Figure S2). Furthermore, we characterized surface area and pore volume of three carbon-coated Si foam particles (no calcination-Si (ncSi), air-calcined-Si (acSi), and oxygen-calcined-Si (ocSi)) (ESI, Figure S3 and S4).

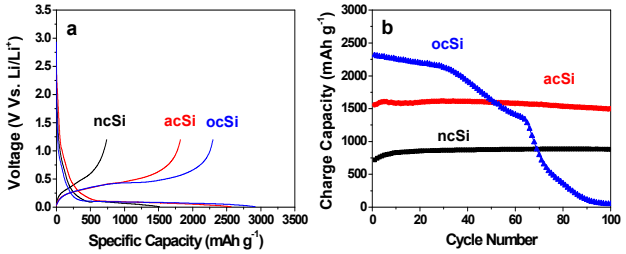

Fig. 2 Electrochemical tests of carbon-coated Si foam particles (ncSi, acSi, and ocSi) prepared by three different calcination processes. (a) First cycle voltage profiles of three samples obtained at 0.05 C rate between 0.005 and 1.2 V. (b) Cycle performances of three Si foam electrodes at 0.2 C (discharge-charge) rate were tested to 100 cycles.

Figure 2a shows the first cycle galvanostatic discharge (lithiation)-charge (delithiation) curves for three carbon-coated Si foam samples at 0.05 C rate in the range of 0.005-1.2 V. The ncSi shows an initial discharge capacity of 1510 mAh g^{-1} and charge capacity of 740 mAh g^{-1}, corresponding to a very low initial coulombic efficiency of 49%. It may be attributed to the formation of SiC layer that can be produced by additional heat generation during the magnesiothermic reduction.[40,41] Crystalline SiC was formed via chemical reduction of SiO_2 as Si source and copolymer surfactant as carbon source as the following reaction: $SiO_2(s) + C(s) + 2Mg(g) \rightarrow SiC(s) + 2MgO(s)$.[40,41] We confirmed the formation of SiC layers in case of ncSi particles by XRD (ESI, Figure S5). Insulating SiC layers formed at the Si surface act as side reaction in the electrochemical cells as Lipson et al. reported previously.[42] In contrast, acSi and ocSi without SiC layers showed an initial discharge (charge) capacities of 2560 (1820) and 2915 (2290) mAh g^{-1}, respectively, with a significant increase of initial coulombic efficiency. In case of acSi sample, even though there is no detection of carbon in the energy-dispersive X-ray spectroscopy (EDS) characterization after calcination, initial coulombic efficiency of the acSi anode was slightly decreased, compared to the ocSi anode.

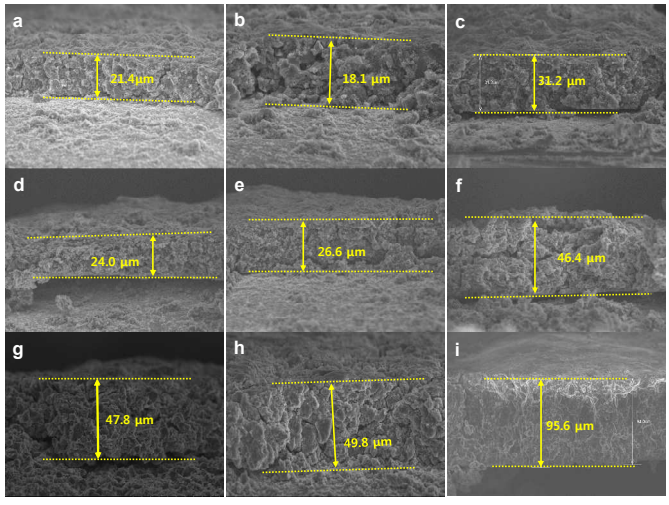

Fig. 3 Cross-sectional SEM images showing volume expansion of three Si electrodes (a-c: as-prepared, d-f: after 1st cycle lithiation, and g-i: after 100th cycle lithiation). Electrode thicknesses of ncSi (a: before, d: 1st cycle, and g: 100th cycle), acSi (b: before, e: 1st cycle, and f: 100th cycle), and ocSi (c: before, f: 1st cycle, and i: 100th

cycle). The ncSi, acSi, and ocSi electrodes showed volume expansion of 120%, 175%, and 212%, respectively, after 100 cycles.

However, the cycling performances of three porous Si anodes show the opposite tendency (Figure 2b). The ocSi, acSi, and ncSi anodes showed charge capacities of 50, 1500, and 850 mAh g^{-1} after 100 cycles at 0.2 C rate (discharge-charge), respectively, corresponding to the capacity retention of 2%, 96%, and 100%. In particular, excellent cycling performances of the acSi electrodes may be explained as follows: (i) a negligible amount of carbon layers in the porous Si formed during the chemical reduction acts as a buffer layer to a large volume change during the cell operation, (ii) carbon-coated Si foam structure also decrease mechanical stress that occurs during the lithiation and delithiation process.

We further investigated volume expansion of ncSi, acSi, and ocSi electrodes after 1st and 100th cycle lithiation. After cycling, the electrodes were carefully disassembled in a glove box. Subsequently, before and after cycling, the thicknesses of three electrodes were measured by cross-sectional SEM (Figure 3). The ncSi, acSi, and ocSi electrodes showed a low volume expansion of 10%, 31%, and 33%, respectively, after 1th cycle lithiation. However, after 100th cycle lithiation, the ncSi, acSi, and ocSi electrodes showed volume expansion of 120%, 175%, and 212%, respectively. From these results, we suggest that residual carbon layers during calcination process of porous SiO_2 particles may affect the cycling retention and the volume expansion of final Si foam electrodes.

3.2. Effect of heat scavenger on the morphology of Si particles

In general, mgnesiothermic reduction reaction between Mg and SiO_2 generates massive heat, resulting in collapses the architecture of SiO_2 particles and agglomeration of as-synthesized Si particles. Won et al. reported that the exothermic temperature measured in the magnesiothermic reduction could reach a very high temperature, 1720 °C.[43] When the magnesiothermic reaction was carried out in solid phase diluted with alkali metal halides (e.g., NaCl, $MgCl_2$, $CaCl_2$, etc.), molten salts can consume the generated heat.[44, 45]

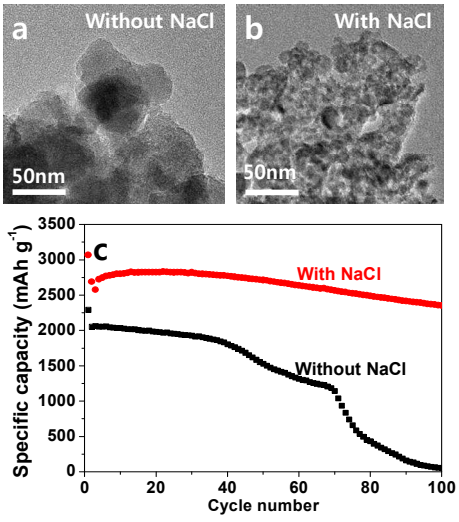

Fig. 4 TEM images of Si foam obtained by magnesiothermic reaction (a) without NaCl and (b) with NaCl. (c) Cycle performances of Si foam electrodes with NaCl (red, solid dot) and without NaCl (black, solid square) were tested at 0.2 C (discharge-charge) until 100 cycles.

We employed NaCl as a heat scavenger to retain the original SiO_2 foam structure after the chemical reduction. The oxygen-calcined SiO_2/NaCl mixture and Mg powder (SiO_2:Mg:NaCl = 1:0.8:1 in mass) were homogeneously mixed together in an argon-filled glovebox. Subsequently, the mixture was heated in a tube furnace at 700 °C for 3 h under argon environment. After the reaction, NaCl salt was washed several times by water and MgO by-products salts were completely removed from 1M HCl. Figure 4a and 4b show TEM images of Si particles synthesized without and with NaCl salts, respectively. As expected, Si particles with void spaces were obtained in the presence of NaCl, while Si obtained in the absence of NaCl was seriously agglomerated. After both Si particles were coated with carbon contents of 8 wt%, they were cycled at 0.2 C rate (discharge-charge) between 0.005 and 1.2 V. Porous Si electrodes (with NaCl) exhibited a high reversible capacity of 2350 mAh g^{-1} after 100 cycles, corresponding to the capacity retention of 87.4% compared to initial capacity. In contrast, Si electrodes (without NaCl) showed a significant capacity decaying (capacity retention of 2.5% after 100 cycles). Similarly, volume expansion of porous Si electrodes (with NaCl) was significantly decreased after 100 cycles, compared to the Si electrodes (without NaCl) (ESI, Figure S6). These results suggested that magnesiothermic reduction in the presence of molten salts reduces exothermic heat, resulting in preservation of original SiO_2 structure and a significant improvement of electrochemical properties of Si electrodes.

3.3. Synthesis of metal-loaded Si foam

Another effective strategy to improve electrochemical properties of Si foam anode is to introduce metal nanoparticles within Si foam, since one of the critical problems related to Si-based particles is their low intrinsic electrical conductivity. We employed well-known silver (Ag) mirror reaction to coat Ag nanoparticles on the surface of oxygen-calcined SiO_2 foam particles.[46] A one-pot chemical reduction of Ag precursor in the presence of n-butylamine led to a formation of Ag-loaded SiO_2 foam particles at room temperature. Typically, 0.25 g of oxygen-calcined SiO_2 foam particles was dispersed into 20 mL of ethanol at 35 °C in a propylene vessel, and subsequently, 50 mM of AgNO3 and 50 mM of n-butylamine were simultanesouly added to the solution and kept stirring for 10 min.

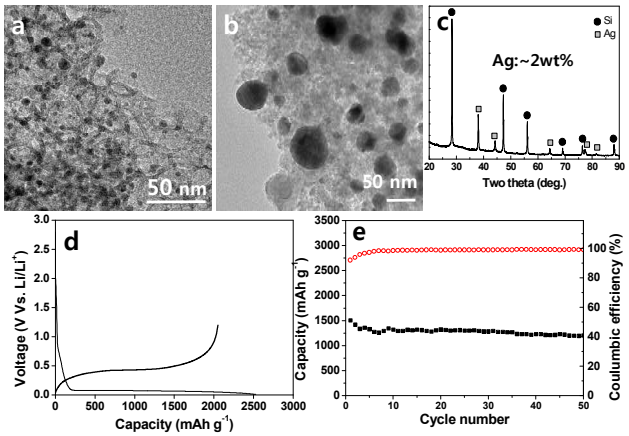

Fig. 5 TEM images of (a) Ag-loaded SiO2 foam and (b) Ag-doped Si particles. (c) XRD patterns of the Ag-doped Si particles show that Ag and Si are crystalline structure. (d) First cycle voltage profile of the Ag-doped Si anode was obtained at 0.05 C rate between 0.005 and 1.2 V. (e) Cycling retention of the Ag-doped Si was obtained at 0.2 C rate (discharge-charge) until 50 cycles.

Figure 5a clearly shows that Ag nanoparticles with diameters of 5-10 nm were uniformly distributed into SiO_2 foam particles without a serious aggregation. Subsequent magnesiothermic reduction of Ag-loaded SiO_2 and Mg vapor led to a successful formation of Ag-doped Si particles. During the chemical reduction process, a significant aggregation of Ag nanoparticles within Si foam was seen due to the exothermic heat. However, the bigger Ag particles were still dispersed well into the Si foam particles (Figure 5b). XRD patterns of the Ag-loaded Si particles indicate that crystalline Ag and Si particles are clearly detected (Figure 5c). Moreover, Ag contents of 2 wt% were confirmed through the EDS analysis. The Ag-doped Si foam electrodes were tested by galvanostatic discharging and charging at a rate of 0.05-0.2 C in the range of 0.005-1.2 V. The first discharge and charge capacities are 2580 and 2085 mAh g^{-1}, respectively, corresponding to the initial coulombic efficiency of 80.8% (Figure 5d). The increasing coulombic efficiency is attributed to the enhancement of electrical conductivity owing to the Ag doping. Subsequent cycling performances were tested at 0.2 C (discharge-charge) rate. After 50 cycles, a high reversible capacity of 1220 mAh g^{-1} was exhibited with a high coulombic efficiency per cycle (>99.5% after 5 cycles). To further investigate the superior electrochemical property of the Ag-doped Si electrodes, electrochemical impedance spectroscopy (EIS) was conducted. The Nyquist impedance plots are obtained after 50th cycle for Ag-doped ncSi and ncSi sample (ESI, Figure S7). The charge-transfer resistance (R_{ct} = 5.71 ohm) of the Ag-doped ncSi electrode is smaller than those of ncSi electrode (R_{ct} = 57.92 ohm) at a rate of 0.2 C. This result indicates that the Ag-doped ncSi electrode is more suitable for the Li^+ diffusion.

Moreover, we extended this idea to Cu-doped Si foam particles. Cu-doped Si foam particles were successfully synthesized and their electrochemical performances including a high reversible capacity (2000 mAh g^{-1} at 0.05 C rate) and a good capacity retention (84.2% after 50 cycles at 0.2 C rate) were exhibited (ESI, Figure S8).

4. Conclusion

We demonstrated three effective strategies for enhancing the electrochemical performances of highly porous Si anode prepared by a magnesiothermic reduction reaction. The first strategy was a conversion of hierarchical SiO_2 to Si with preserving the original SiO_2 porous structure. By controlling calcination process, amount of residual carbon sources in as-prepared porous SiO_2 was controlled by tuning the calcination process. Subsequent Si particles obtained by magnesiothermic reaction showed different electrochemical performances. The second way was to introduce heat scavenging molten salt during magnesiothermic reduction to minimize exothermic heat. It led to a successful synthesis of shape-preserving Si foam particles after the chemical reduction, resulting in a significant improvement of cycling retention. The third strategy is to introduce metal nanoparticles within Si foam particles during the chemical reduction reaction. Electrically conductive Ag and Cu nanoparticles were uniformly dispersed in Si foam, leading to the significant improvements of initial coulombic efficiency and cycle retention of metal-doped Si anodes. These strategies can be extended not only Si particles but also other particles for improving electrochemical performances for practical rechargeable battery applications.

Acknowledgements

This work was supported by the MSIP (NIPA-2013-H0301-13-1009) program.

Notes and references

[a] School of Energy and Chemical Engineering, Ulsan National Institute of Science and Technology (UNIST), 50 UNIST-gil, Ulju-gun, Ulsan 689-798, Republic of Korea
E-mail: spark@unist.ac.kr
[b] Duksan Hi-metal company, Yeonam-Dong, Buk-gu,Ulsan 683-804, Korea

1 G.-A. Nazri and G. Pistoia, *Lithium Batteries: Science and Technology*. Kluwer Academic/Plenum, Boston, 2004.
2 M. S. Whittingham, *MRS Bull,* 2008, **33**, 411.
3 M. Armand and J. M. Tarascon, *Nature,* 2008, **451**, 652.
4 C. Liu, F. Li, L.-P. Ma and H.-M. Cheng, *Adv. Mater.* 2010, **22**, E28.
5 M.-K. Song, S. Park, F. M. Alamgir, J. Cho and M. Liu, *Mater. Sci. Eng. R*, 2011, **72**, 203.
6 J. R. Szczech and S. Jin, *Energy Environ. Sci,*. 2011, **4**, 56.
7 M. N. Obrovac and L. Christensen, *Electrochem. Solid-State Lett,*. 2004, **7**, A93.
8 S. Hossain, Y. K. Kim, Y. Saleh and R. Loutfy, *J. Power Sources,* 2003, **114**, 264.
9 B. A. Boukamp, G. C. Lesh and R. A. Huggins, *J. Electrochem. Soc,*. 1981, **128**, 725.
10 U. Kasavajjula, C. Wang and A. J. Appleby, *J. Power Sources,* 2007, **163**, 1003.
11 T. L. Kulova, Y. V. Pleskov, A. M. Skundin, E. I. Terukov and O. I. Kon'kov, *Russ. J. Electrochem.*, 2006, **42**, 708.
12 S. R. Chen, M. L. Gordin, R. Yi, G. Howlett, H. Sohn and D. H. Wang, *Phys. Chem. Chem. Phys.*, 2012, **14**, 12741.
13 J. Cho, *J. Mater. Chem.,* 2010, **20**, 4009.
14 A. Gohier, B. Laïk, K.-H. Kim, J.-L. Maurice, J.-P. Pereira-Ramos, C. S. Cojocaru and P. T. Van, *Adv. Mater.*, 2012, **24**, 2592.
15 X. Zhou, Y.-X. Yin, L.-J. Wan and Y.-G. Guo, *Chem. Commun.*, 2012, **48**, 2198.
16 H. Jia, P. Gao, J. Yang, J. Wang, Y. Nuli and Z. Yang, *Adv. Energy Mater.*, 2011, **1**, 1036.
17 F.-H. Du, K.-X. Wang, W. Fu, P.-F. Gao, J.-F. Wang, J. Yang and J.-S. Chen, *J. Mater. Chem. A*, 2013, **1**, 13648.
18 C. K. Chan, H. Peng, G. Liu, K. McIlwrath, X. F. Zhang, R. A. Huggins and Y. Cui, *Nat. Nanotech*., 2008, **3**, 31.
19 R. Mukherjee, R. Krishnan, T.-M. Lu and N. Koratkar, *Nano Energy*, 2012, **1**, 518.
20 R. Yi, F. Dai, M. L. Gordin, S. Chen and D. Wang, *Adv. Energy Mater.*, 2013, **3**, 295.
21 P. G. Bruce, B. Scrosati and J.-M. Tarascon, *Angew. Chem. Int. Ed.*, 2008, **47**, 2930.
22 A. Manthiram, A. Vadivel Murugan, A. Sarkar and T. Muraliganth, *Energy Environ. Sci.,* 2008, **1**, 621.
23 B. M. Bang, H. Kim, H.-K. Song, J. Cho and S. Park, *Energy Environ. Sci.*, 2011, **4**, 5013.
24 A. Magasinski, P. Dixon, B. Hertzberg, A. Kvit, J. Ayala and G. Yushin, *Nat. Mater.,* 2010, **9**, 353.
25 B. M. Bang, J.-I. Lee, H. Kim, J. Cho and S. Park, *Adv. Energy Mater.*, 2012, **2**, 878.
26 H. Kim, B. Han, J. Choo and J. Cho, *Angew. Chem., Int. Ed.*, 2008, **47**, 10151.
27 S. Yoo, J.-I. Lee, M. Shin and S. Park, *ChemSusChem*, 2013, **6**, 1153.
28 Y. Yu, L. Gu, C. Zhu, S. Tsukimoto, P. A. van Aken and J. Maier, *Adv. Mater.*, 2010, **22**, 2247.
29 J.-I. Lee, K. T. Lee, J. Cho, J. Kim, N.-S. Choi and S. Park, *Angew. Chem. Int. Ed.*, 2012, **51**, 2767.
30 D. Chen, X. Mei, G. Ji, M. Lu, J. Xie, J. Lu and J. Y. Lee, *Angew. Chem. Int. Ed.*, 2012, **51**, 2409.
31 H. Jia, P. Gao, J. Yang, J. Wang, Y. Nuli and Z. Yang, *Adv. Energy Mater.,* 2011, **1**, 1036.
32 H. Kim, J. C. Jung, P. Kim, S. H. Yeom, K.-Y. Lee and I. K. Song, *J. Mol. Catal. A*, 2006, **259**, 150.
33 D. Zhao, J. Feng, Q. Huo, N. Melosh, G. H. Fredrickson, B. F. Chmelka and G. D. Stucky, *Science*, 1998, **279**, 548.

34 H. Minakuchi, K. Nakanish, N. Soga, N. Ishizuka and N. Tanaka, *Anal. Chem.,* 1996, **68**, 3498.
35 J. Lee, J. Kim, J. Kim, H. Jia, M. I. Kim, J. H. Kwak, S. Jin, A. Dohnalkova, H. G. Park, H. N. Chang, P. Wang, J. W. Grate and T. Hyeon, *Small*, 2005, **1**, 744.
36 M. E. Davis, *Nature,* 2002, **417**, 813.
37 F. Hoffmann, M. Cornelius and J. Morell, *Angew. Chem. Int. Ed.*, 2006, **45**, 3216.
38 I. I. Slowing, B. G. Trewyn, S. Giri and V. S.-Y. Lin, *Adv. Funct. Mater.*, 2007, **17**, 1225.
39 Z. Bao, M. R. Weatherspoon, S. Shian, Y. Cai, P. D. Graham, S. M. Allan, G. Ahmad, M. B. Dickerson, B. C. Church, Z. Kang, H.W. Abernathy III, C. J. Summers, M. Liu and K. H. Sandhage, *Nature*, 2007, **446**, 172.
40 Y. Shi, F. Zhang, Y.-S. Hu, X. Sun, Y. Zhang, H. L. Lee, L. Chen and G. D. Stucky, *J. Am. Chem. Soc.*, 2010, **132**, 5552.
41 S. Choi, J. C. Lee, O. Park, M.-J. Chun, N.-S. Choi and S. Park, *J. Mater. Chem. A*, 2013, **1**, 10617.
42 A. L. Lipson, S. Chattopadhyay, H. J. Karmel, T. T. Fister, J. D. Emery, V. P. Dravid, M. M. Thackeray, P. A. Fenter, M. J. Bedzyk and M. C. Hersam, *J. Phys. Chem. C*, 2012, **116**, 20949.
43 C. W. Won, H. H. Nersisyan and H. I. Won, *Sol. Energy Mater. Sol. Cell.*, 2011, **95**, 745.
44 C. W. Won, H. H. Nersisyan, H. I. Won and J. H. Lee, *Curr. Opin. Solid State Mater. Sci.*, 2010, **14**, 53.
45 W. Luo, X. Wang, C. Meyers, N. Wannenmacher, W. Sirisaksoontorn, M. M. Lerner and X. Ji, *Sci. Rep.*, 2013, **3**, 2222.
46 S. Yoo, J.-I. Lee, S. Ko and S. Park, *Nano Energy*, 2013, **2**, 1271.

